Exp. Theo. NANOTECHNOLOGY 5 (2021) 39 – 54 https://doi.org/10.56053/5.3.39

Modeling of electronic structure for dome-shaped quantum dots

A. Subhi[1,*], *M. A. Saeed*[2]

[1]Physics Department, Science College, Al-Muthana University, Samawah, Iraq
[2]Department of Physics, Division of Science & Technology, University of Education, Lahore, Pakistan
[*]) E-mail: ahmedsbhe@yahoo.com

Received 2/3/2021, *Accepted* 9/6/2021, *Published* 15/9/2021

A Hamiltonian operator in assessing the energy levels and wavefunctions of quantum dots (QDs) was proposed. The finite element method was used to solve the numerical Schrödinger equation for envelope function in the effective mass approximation. Within this model, we have investigated QDs with different geometries (cone, lens and dome-shaped dot). While it is easy to attain stability for conical QDs, it is difficult with lens QDs. Strain and mole-fraction effects are also studied. Our results coincide with the experimental one.

Keywords: Quantum dot; Hamiltonian; Effective Mass Approximation; Strain and mole-fraction effects; MATHLAB; Wurtzite III-nitride semiconductors.

1. INTRODUCTION

Quantum dots (QDs) are zero-dimensional semiconductor nanostructures having discrete energy levels, like “artificial atoms” [1]. The electronic structure is vital to understand the QDs behavior in a particular system. The optical properties also depend on the electronic structure Many theories are discussing the electronic properties of QDs. According to such theories, electronic properties mainly depend on the shapes of these semiconductor nanocrystals, which have been observed experimentally, but the perfect calculation of QD structure has not yet been realized due to manufacturing imperfections, which results from growth methods. One of these theories i.e. k.p theory gives a complete description of electronic structure, but due to its high computational requirements as it requires knowing the structure parameters. There are many analytical and numerical models discussing QD electronic structure with enough adequacy and reliability with the experimental observations. For example, Jungho and Chuang [2] prefer the quantum disk model, Zhang, Shi [3] discusses cylindrical QDs, Nenad, Zoran [4] presents a case when QDs are in the form of a truncated hexagonal pyramid, and truncated cone dots are discussed by Saidi et al. [5].

During the last decade, several studies have concentrated on III-nitride semiconductor materials for applications in short-wavelength light sources, as well as for high-power or high-speed electron devices. Wurtzite crystal of III-nitride is a direct bandgap semiconductor, and it has many individual properties including wide bandgaps, high-saturation velocity, effects of strong excitonic, and high absorption and radiation coefficients [6].

In this study, we develop a new Hamiltonian for different shapes of QDs such as cone, and lens or dome shape. In this Hamiltonian, we can solve three or two-dimensional geometry problem, which needs extensive numerical effort by reducing it to one dimension problem. The finite element method (FEM) is used to calculate the eigenvalues of electron energy corresponding to the QDs system, and we have also found the conduction and valence subbands with and without strain.

2. HAMILTONIAN AND COMPUTATIONAL METHODS

To probe the properties of semiconductor QDs with cone, lens, or dome shape, the effective mass approximation (EMA) of one-band Schrodinger equation for electrons (holes) in conduction (valence) bands can be written as

$$H\Psi(\rho,\varphi) = E\Psi(\rho,\varphi) \tag{1}$$

and the Hamiltonian of the system

$$H = -\frac{\hbar^2}{2m^*}\nabla^{2,n} + V \tag{2}$$

where

$$V = \begin{cases} 0 & \rho \le r \\ V_B & \rho > r \end{cases} \tag{3}$$

and

$$m = \begin{cases} m_d^* & \rho \le r \\ m_W^* & \rho > r \end{cases} \tag{4}$$

where ħ is Planck's constant divided by 2π, m* is the effective mass of electron or hole (m_d^* for QD and m_w^* for wetting layer (WL), V is the potential energy determined by the conduction or valence band offset (0 inside dot, and VB outside dot (in the WL)), $\Psi(\rho,\varphi)$ and E is the wave function and their corresponding quantized energy levels, respectively. Here ρ is the radial coordinate, and φ is the azimuthal angle ranging between (0–2π). The square of the del operator ($\nabla^{2,n}$) is obtained in a form depending on the shape of the dot, where n representing the geometrical factor, it is (1 for cone shape, and 2 for lens or dome shape), and r and h are radius and height for the cone, lens or dome shape, respectively, as shown in Figure1.

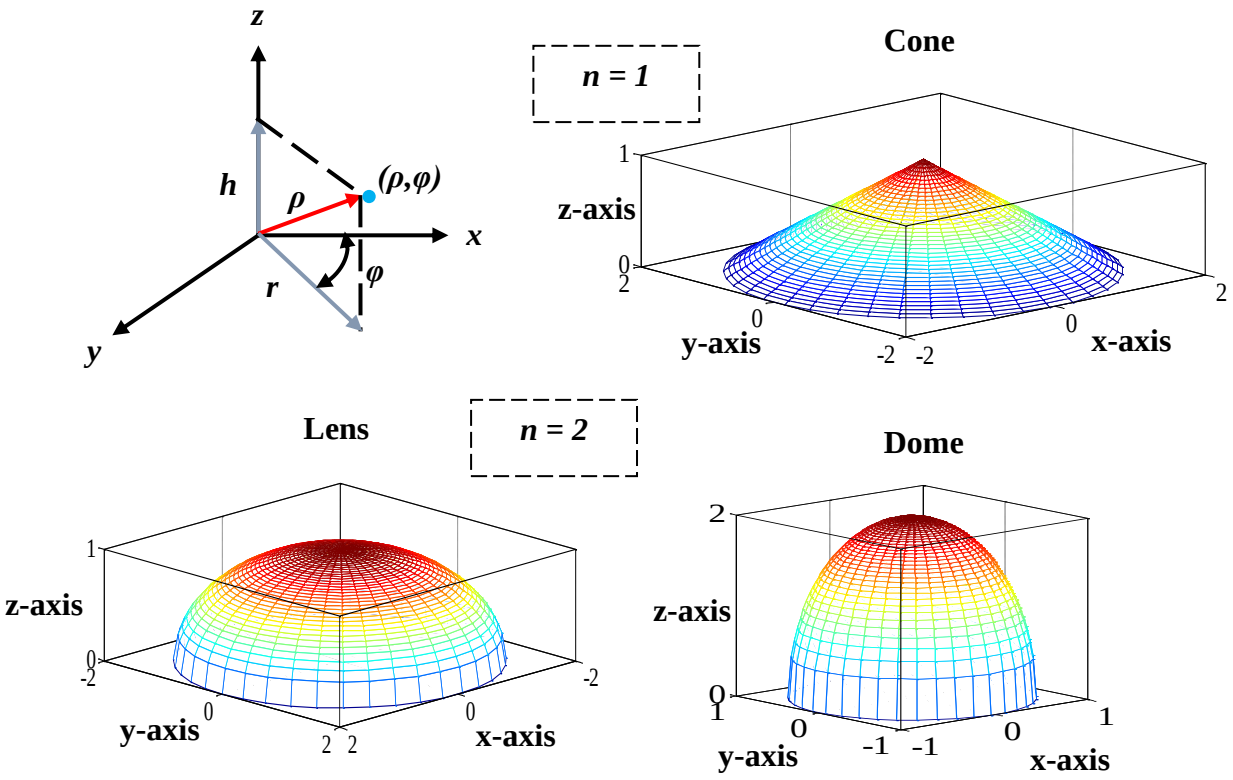

Figure 1 The shapes of QD can be modeled by basis functions used in this novel operator.

We start with the Laplace operator in Cartesian coordinates and transform it into ρ, φ coordinates, to consider the cone, lens or dome-shaped QD, by using the following relations

$$z = h\left(1-\left(\frac{\rho}{r}\right)^{n}\right)^{\frac{1}{n}}$$

where $x = \rho\cos\varphi$, $y = \rho\sin\varphi$, and

where $0 \le \varphi \le 2\pi$, $0 \le \rho \le r$, and r, h represents the radius and height of the shape, respectively. Then $\nabla^{2,n}$ is redefined in ρ, φ coordinates by;

$$\nabla^{2,n} = \left(1+\frac{r^2}{h^2}\rho^{2(1-n)}\left(r^n-\rho^n\right)^{2(1-\frac{1}{n})}\right)\frac{\partial^2}{\partial\rho^2}+\left(\frac{1}{\rho}+(1-n)\frac{r^{2+n}}{h^2}\rho^{1-2n}\right.$$

$$\left.\left(r^n-\rho^n\right)^{(1-\frac{2}{n})}\right)\frac{\partial}{\partial\rho}+\frac{1}{\rho^2}\frac{\partial^2}{\partial\varphi^2} \qquad (5)$$

QD structure with cylindrical symmetry is assumed using the separation of variables. Then, the wavefunction $\Psi(\rho,\varphi)$ can be separated into two parts.

$$\Psi(\rho,\varphi) = R(\rho)\Phi(\varphi) \tag{6}$$

Substitute Eq's. (2 - 6) into Eq. (1), multiply by $\frac{-2m^*\rho^2}{\hbar^2 R(\rho)\Phi(\varphi)}$, and rearrange to get

$$\left\{\left(1+\frac{r^2}{h^2}\rho^{2(1-n)}\left(r^n-\rho^n\right)^{2(1-\frac{1}{n})}\right)\frac{\rho^2}{R(\rho)}\frac{\partial^2 R(\rho)}{\partial\,\rho^2}+\left(1+(1-n)\frac{r^{2+n}}{h^2}\rho^{1-2n}\right.\right.$$

$$\left.\left.\left(r^n-\rho^n\right)^{(1-\frac{2}{n})}\right)\frac{\rho}{R(\rho)}\frac{\partial R(\rho)}{\partial\rho}\right\}+\frac{2m^*}{\hbar^2}(E-V)\rho^2=\frac{-1}{\Phi(\varphi)}\frac{\partial^2\Phi(\varphi)}{\partial\varphi^2} \tag{7}$$

The last term in Eq. (7) is a function of φ only, which immediately can be assumed as a constant (ℓ), then

$$\frac{1}{\Phi(\varphi)}\frac{\partial^2\Phi(\varphi)}{\partial\varphi^2}=-\ell^2 \tag{8}$$

ℓ is an integer. Using the same boundary conditions in a finite well, we have a solution of the form

$$\Phi_\ell(\varphi)=\begin{cases}C_1 e^{i\ell\varphi}\\ C_2 e^{-i\ell\varphi}\end{cases}$$

normalizing to find C1and C2, we get

$$\Phi_\ell(\varphi)=\frac{1}{\sqrt{2\pi}}e^{i\ell\varphi} \tag{9}$$

where ℓ=0,±1,±2, …

Changing the part that containing φ in Eq. (7) and rewriting to become

$$-\left(1+\frac{r^2}{h^2}\rho^{2(1-n)}\left(r^n-\rho^n\right)^{2(1-\frac{1}{n})}\right)\frac{\partial^2 R_\ell(\rho)}{\partial\,\rho^2}-\left(\rho^{-1}+(1-n)\frac{r^{2+n}}{h^2}\rho^{1-2n}\right.$$

$$\left.\left(r^n-\rho^n\right)^{(1-\frac{2}{n})}\right)\frac{\partial R_\ell(\rho)}{\partial\rho}+\ell^2\rho^{-2}R_\ell(\rho)=p^2R_\ell(\rho) \tag{10}$$

where p is a constant define as $p=\sqrt{2m^*(E-V)}/\hbar^2$. The last equation represents a simplified Schrodinger equation with any geometric shape (n-factor) and its second-order differential equation with one variable ρ. It can be used to discuss the QD structure at any shape by choosing the order of n, as we do in the following subsections.

2.1. Quantum Cone Model

For a conical quantum dot (CQD) with radius r and height h, the Schrödinger equation for a cone shape, n=1, we use Eq. (10),

$$\rho^2\left(1+\left(\frac{r}{h}\right)^2\right)\frac{\partial^2 R_\ell(\rho)}{\partial\rho^2}+\rho\frac{\partial R_\ell(\rho)}{\partial\rho}+(p^2\rho^2-\ell^2)R_\ell(\rho)=0 \quad (11)$$

We can solve Eq. (11) numerically by using FEM.

2.2 Quantum Lens or Dome Model

For a lens-shaped quantum dot (LQD) or dome-shape quantum dot (DQD) with radius r and height h the Schrödinger equation with (n=2), using Eq. (10), is given by

$$\left(\rho^2+\frac{r^2}{h^2}\left(r^2-\rho^2\right)\right)\frac{\partial^2 R_\ell(\rho)}{\partial\rho^2}+\left(\rho-\frac{r^4}{h^2}\rho^{-1}\right)\frac{\partial R_\ell(\rho)}{\partial\rho}+\left(p^2\rho^2-\ell^2\right)R_\ell(\rho)=0 \quad (12)$$

There is no analytical solution for this equation; we must go to the numerical solution to find the eigenvalues.

3. NUMERICAL SOLUTION

Although FEM is more difficult to implement than the finite difference method, it is a more flexible method to approximate the partial differential equations. For instance, FEM can easily be extended to higher-order approximations and can be used for very complex geometries [7, 8]. We focus here on the one-dimensional case, and our equations become

$$-f_1(x)\frac{d^2}{dx^2}y(x)+f_2(x)\frac{d}{dx}y(x)+f_3(x)y(x)=\lambda f_4(x)y(x) \quad (13)$$

where $f_1(x)$, $f_2(x)$, $f_3(x)$ and $f_4(x)$ are functions of x, and λ is the eigenvalue. FEM involves the following steps:

a. Divide the domain Ω to the number of linear elements Ne, which are non-overlapping elements Ω_e, where $e=1,...,Ne,$ the global nodes are defined by
x_i, where $i=1,...,Nn$
The total number of nodes is
$Nn=Ne+1$
All two neighboring nodes make one element, this is called a uniform mesh of linear elements, and then the size of each element (he) is the distance between two boundary nodes of the element.
$h_e=x_{i+1}-x_i$

b. We use a weak form for our differential equation,
$\int_\Omega W\ L(y(x))dx=\lambda f_4(x)\int_\Omega W\ y(x)dx$

where L is a differential operator-specific in our problem, and the elemental weak form as

$$\int_{x_i}^{x_{i+1}} W \quad L(y(x))\,dx = \lambda f_4(x) \int_{x_i}^{x_{i+1}} W \quad y(x)\,dx$$

The elemental system will take the form

$$[K^e]\{y\} = [F^e]\{y\} + \{Q^e\} \tag{14}$$

where $\{Q^e\}$ represents boundary conditions vector

c. We approximate the function y^e for each element by using shape functions

$$y^e = \sum_{j=1}^{NnN} y_j^e N_j^e \tag{15}$$

where y_j^e is a nodal unknown at elements jth node, and N_j^e is the shape or basis functions, which are simple piecewise polynomials, and have the Kronecker-Delta δ_{ij} property.

$$N_j^e(x_i) = \delta_{ij}$$

NnN is a number of element nodes (it is equal to 2 for linear elements) see figure 2 (a). Then the shape functions become

$$N_1^e = \frac{x_2 - x}{h_e} \text{ and } N_2^e = \frac{x - x_1}{h_e}$$

But these shape functions have some difficulties, for each element, there will be different functions of x and integration over an element will have limits of x_1^e and x_2^e, which are not appropriate for Gauss Quadrature (GQ) integration. The cure is to use the concept of the master element.

d. For one-dimension linear element, there is only a single master element with local coordinate ζ and length (equal to 2), Figure 2 (b), which are suitable for GQ.

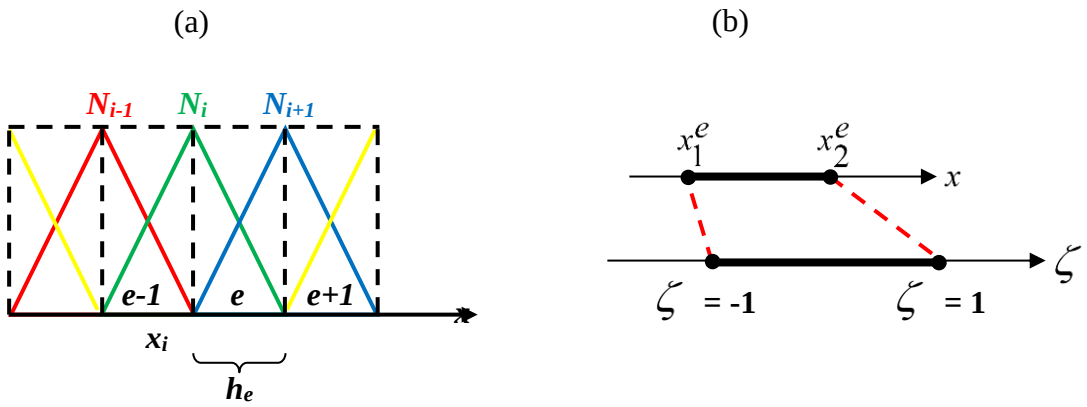

Figure 2 a) Linear basis functions for a 5 node. b) Convert from the actual element to the master element.

To rewrite all integrals by using the term ζ , we must find the relation between global coordinate x and local coordinate ζ . By applying the fact that endpoints of the actual element coincide with those of the master element, we get

$$x = \frac{h_e}{2}\zeta + \frac{x_1^e + x_2^e}{2}$$

and the shape functions

$$N_1^e = \frac{1-\zeta}{2} \text{ and } N_2^e = \frac{1+\zeta}{2}$$

And Jacobian of each element is the ratio of actual elements length to the length of the master element.

$$J^e = \frac{h_e}{2} = \frac{dx}{d\zeta}$$

After performing all these steps Eq. (13) becomes

$$\sum_{-1}^{1} \left\{ f_1(\zeta)\frac{dN_j}{d\zeta}\frac{1}{J^e}\frac{dN_i}{d\zeta}\frac{1}{J^e} + f_2(\zeta)N_i\frac{dN_j}{d\zeta}\frac{1}{J^e} + f_3(\zeta)N_iN_j \right\} J^e d\zeta y_j^e =$$

$$\sum_{-1}^{1} \left\{ f_4(\zeta)N_iN_j \right\} J^e d\zeta y_j^e + Q_i^e \qquad (16)$$

The limits [-1,1] are suitable for GQ integration, which can convert from integration to summation

$$\int_{-1}^{1} g(\zeta)d\zeta = \sum_{k=1}^{NGP} g(\zeta_k)W_k$$

where ζ_k is a coordinate of GQ points, W_k is GQ weights, and NGP is a number of GQ points (in our case equal 3), then

$$\zeta_k = \begin{vmatrix} \sqrt{3/5} \\ 0 \\ -\sqrt{3/5} \end{vmatrix} \text{ and } W_k = \begin{vmatrix} 5/9 \\ 8/9 \\ 5/9 \end{vmatrix}$$

By using matrix form our equations system take the form

$$[K_{ij}^e]\{y\} = [F_{ij}^e]\{y\} + \{Q_{ij}^e\} \qquad (17)$$

To examine our proposed model, we consider an example of one dimension Laplace's equation. It is a simple example for the eigenvalue problem, for the interval [0,π]

$$-u''(x) = \lambda u(x) \qquad (18)$$

at the condition $u(0) = u(\pi) = 0$

It has an analytical solution for the eigenfunction and eigenvalues

$u_k(x) = \sin(kx) = 0$ and $\lambda_k = k^2$

where $k = 1,2,3,...$

By using our model, we find the first five eigenvalues with a different number of elements Ne as given in Table 1. There is a good agreement with the analytical results.

Table 1 Eigenvalues calculated using the model in Eq. (13) with different values of *Ne*.

Exact Value	Computed Value			
	Ne =10	*Ne* =50	*Ne* =100	*Ne* =500
1	0.9844	0.9995	0.9999	1.0000
4	3.5690	3.9900	3.9977	3.9999
9	5.9615	8.9340	8.9870	8.9996
16	8.1296	15.6826	15.9501	15.9986
25	13.1601	23.5258	24.8401	24.9964

4. STRAIN EFFECT

When a material grows on another material (i.e. on a substrate), some strain will appear due to different interatomic distances at, and nearby, the interface between both materials. If the strain gets too big, defects arise from the material. For example, cracks may form within the newly deposited material [9]. As one would expect the further away from the interface, the particular less the deflection from bulk interatomic distances, and hence decreasing the strain. Just one then expects strain to existing throughout the quantum dot interfaces, lessening as one move away on the interfaces.

In this study, the strain effect will be included to lead to changing the confinement energy for both electrons and holes. The strain simply causes energy shifting for the conduction and the valence band edges as below [10-12]

$$\Delta E_c = 2a_c\left(\frac{C_{11}-C_{12}}{C_{11}}\right)\varepsilon \tag{19}$$

$$\Delta E_v = \left(-2a_v\frac{C_{11}-C_{12}}{C_{11}} + b\frac{C_{11}+2C_{12}}{C_{11}}\right)\varepsilon \tag{20}$$

where a_c, a_v, b, C_{11}, C_{12} are the hydrostatic deformation potential for conduction and valence bands, biaxial deformation potential, the elastic stiffness constants, respectively, and ε is the elastic strain comes from lattice mismatch, a_{QD} and a_{WL} are the lattice constants for QD and WL, respectively

$$\varepsilon = \frac{a_{QD}-a_{WL}}{a_{WL}} \tag{21}$$

5. RESULTS AND DISCUSSION

By using MATLAB, we have written a program and employed the parameters listed in Table 2. We have calculated energy levels for QDs of different shapes specifying some of the parameters listed in Table 2 depending on the relations in [13,14]. Figure 3 shows the conduction and valence subbands for CQD. A dense width of subbands is shown for low *In* mole-fraction. The conduction subbands are denser than the valence subbands. With increasing the *In* mole fraction, the valence subbands become denser. After x=0.1 mole fraction, the conduction subbands start appearing including strain shifts subbands to higher energies and more states are recognized.

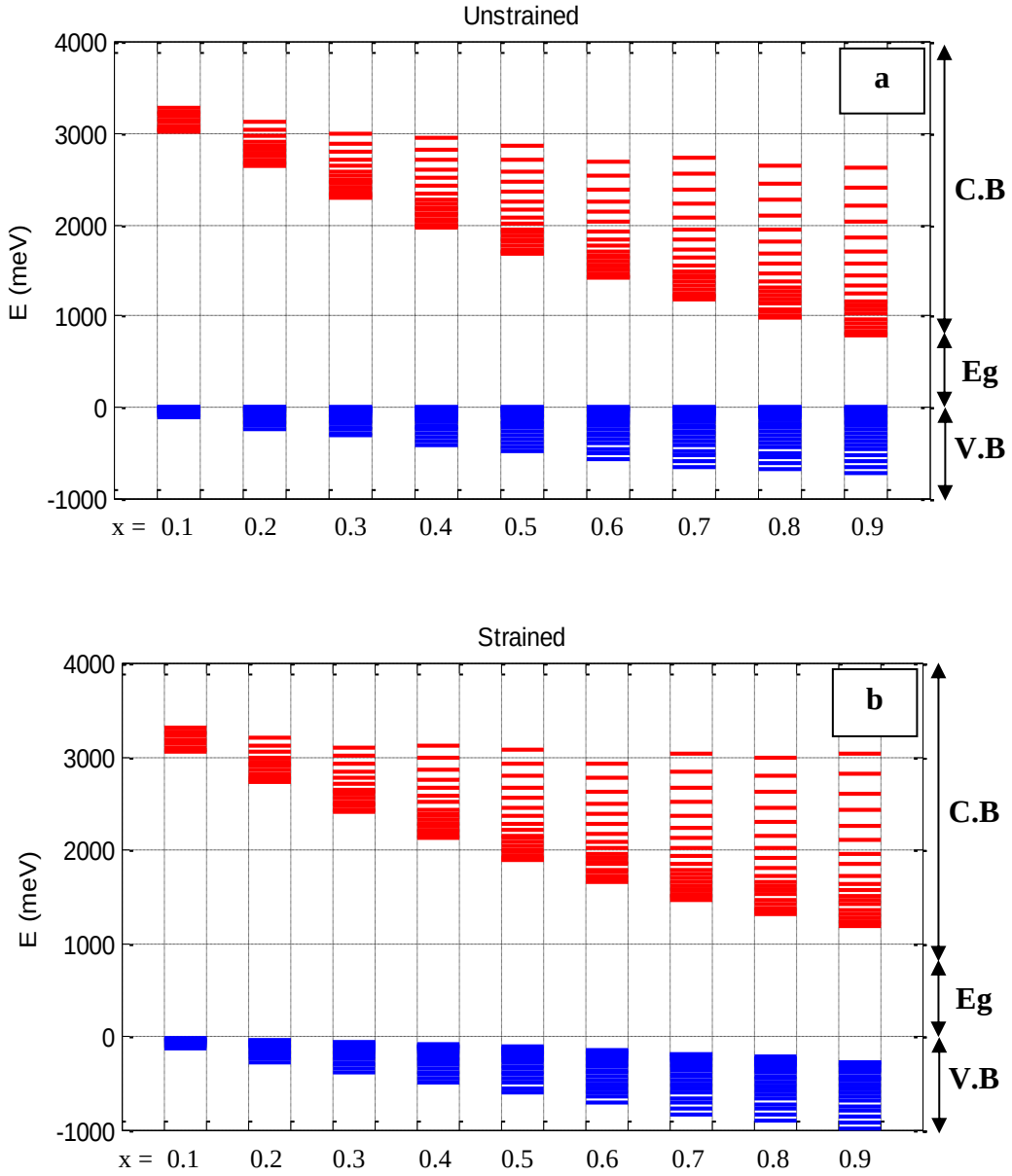

Figure 3 Conduction and valence sub-bands for $In_xGa_{1-x}N/GaN$ structure with changing In- content in QD, a) Unstrained. b) Strained. CQD with r=8.5 nm, h=2.2 nm, and element number Ne=50.

Figure 4 shows the effect of elements number on the calculated energies, where it shows a consistency of the results obtained. This can also be seen in Table 1. It is shown that after 70 elements the results are stable for CQD as in figure 4 (a) where it is easy to attain stability while for LQD the situation is different. In LQD, the situation strongly depends on the element size (*he*). When we take it as 250, figure 4 (b), it is impossible to attain stability while reducing the element size to 100, a good stability is attained after 300 elements as shown in figure 4 (c).

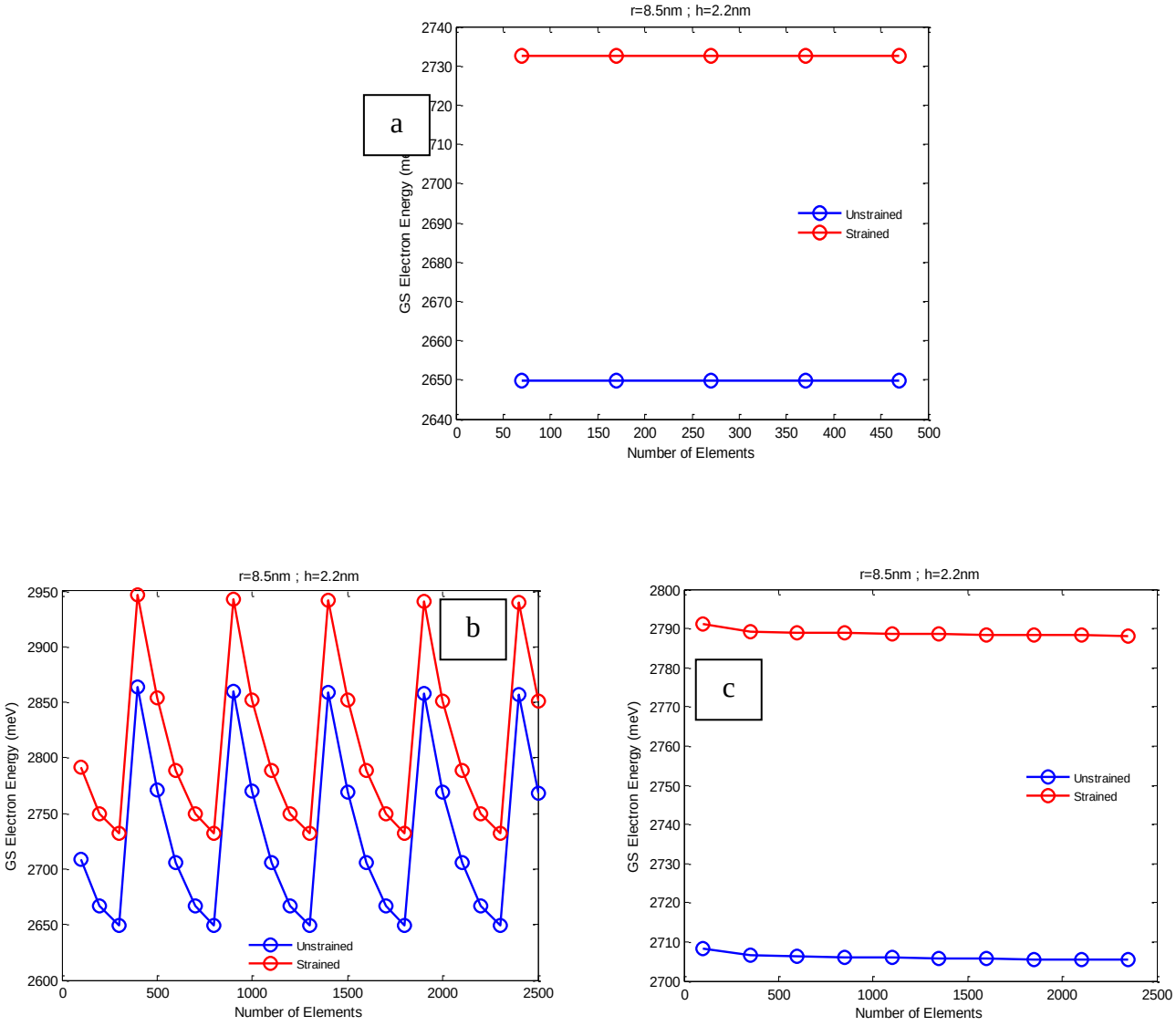

Figure 4 Calculating ground state (GS) electron energy vs a number of elements for $In_{0.2}Ga_{0.8}N/GaN$ strained and unstrained QD structures with r=8.5 nm, h=2.2 nm for a) CQD, b) LQD with the size of the element was 250, and c) LQD with the size of the element was reduced to 100.

Figure 5 shows the quantum size effect where the radius effect is shown at 2.2nm QD height for both strained and unstrained structures where the transition energy between the 1st excited states (ES) increases linearly with radius. Inclusion of the strain in the calculations shifts the transition energy

upward by approximately 40meV. Figure 5 (b) shows the effect of the QD height on the transition energy of the first two subbands which show a prominent effect at QD heights until approximately 2 nm. While the transition energy increases with QD radius, it reduces with QD height. Height is shown to be somewhat efficient than radius in changing subbands.

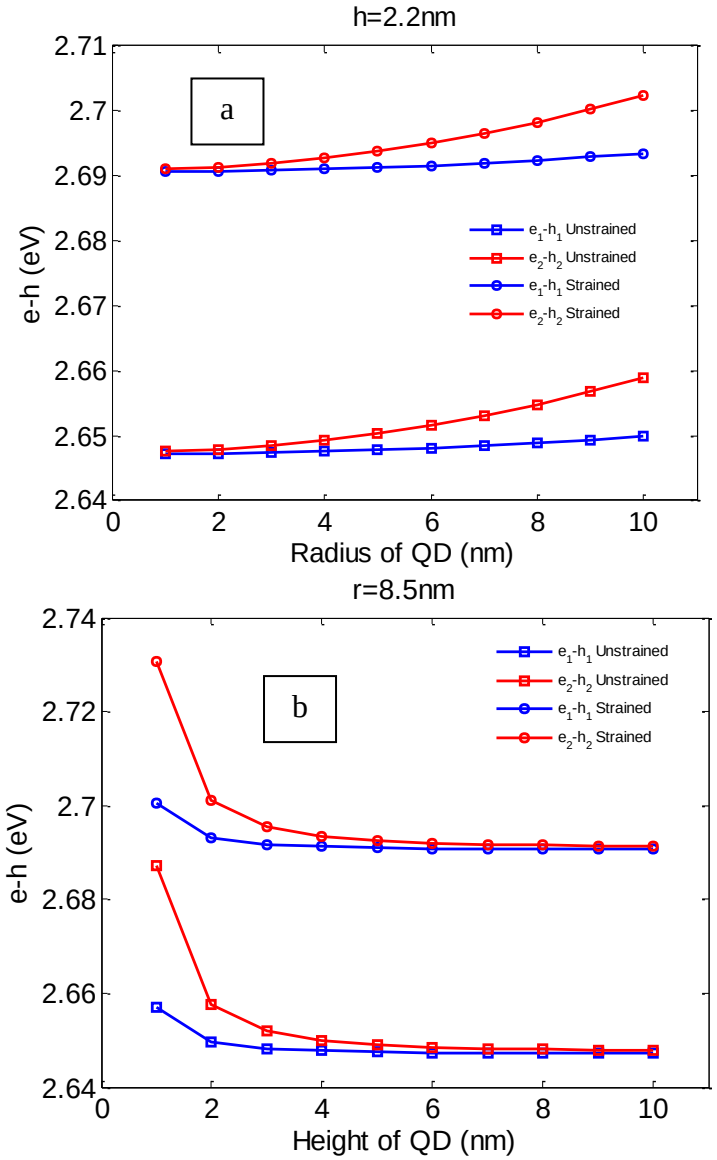

Figure 5 The electron-hole transition energy for GS $(e_1 - h_1)$ and first ES $(e_2 - h_2)$ of CQD as a function of, a) QD radius, b) QD height. The structure is $In_{0.2}Ga_{0.8}N/GaN$.

Table 2 Material parameters of wurtzite III-nitride semiconductors [13,14].

Parameter	*Notation*	Unit	InN	GaN	$In_xGa_{1-x}N$
Electron effective mass	m_e	kg	$0.11m_o$[a]	$0.22m_o$	0.22 - 0.11x
Hole effective mass	m_h	kg	$0.5m_o$	$0.8m_o$	0.8 – 0.3x
Lattice constant	a	A°	3.545	3.189	3.189 + 0.356x
Band gap energy	E_g	eV	0.64	3.434	$3.434 - 4.225x + 1.43x^2$
Crystal field split energy	$\Delta_1 = \Delta_{cr}$	eV	0.024	0.01	0.01 + 0.014x
Spin-orbit split energy	$\Delta_2 = \Delta_3$	eV	0.005	0.017	0.017 – 0.012x
Dielectric constant	ε_r	-	15	9.6	9.6 + 5.4x
Refractive index	$n_b=\sqrt{\varepsilon_r}$	-	3.87	3.09	3.09 + 0.78x
Elastic constant	C_{11}	GPa	223	390	390 – 167x
Elastic constant	C_{12}	GPa	115	145	145 – 30x
Hydrostatic deformation potential for conduction band	a_c	eV	-2.65	-6.71	4.06x – 6.71
Hydrostatic deformation potential for valence band	a_v	eV	-0.7	-0.69	- (0.69 + 0.01x)
Biaxial deformation potential	b	eV	-1.2	-2	0.8x - 2

Figure 6 shows the conduction and valence subbands for LQD. Separated subbands appear for both conduction and valence subbands. Including strain shifts, subbands to higher energies and more states are recognized. Compared with figures related to the cone shape, these figures show size effect where states are separated obviously compared with CQD states. Figure 7 shows the quantum size effect on LQD where e-h transition energy versus QD radius is shown in figure 7 (a) while the lens height effect is shown in figure 7 (b). Reducing QD height or increasing radius is more efficient. This with results obtained from others [2]. However, the size effect in the case of LQD is more efficient than the case of CQD. When QD radius changes from 2-10nm, the transition energy increases from 2.65eV to 2.79eV for unstrained structure and 2.84eV for strained structure i.e. it changes by 0.14eV while for the case of CQD it increases by not more than 0.015eV. Thus, LQD transition energy increases by one order of magnitude compared with CQD. Figure 8 shows the consistency of our results with experiments for a similar structure in [14]. Another comparison with experimental results is also shown in figure 9, where the results agree with the experimental one obtained in [15].

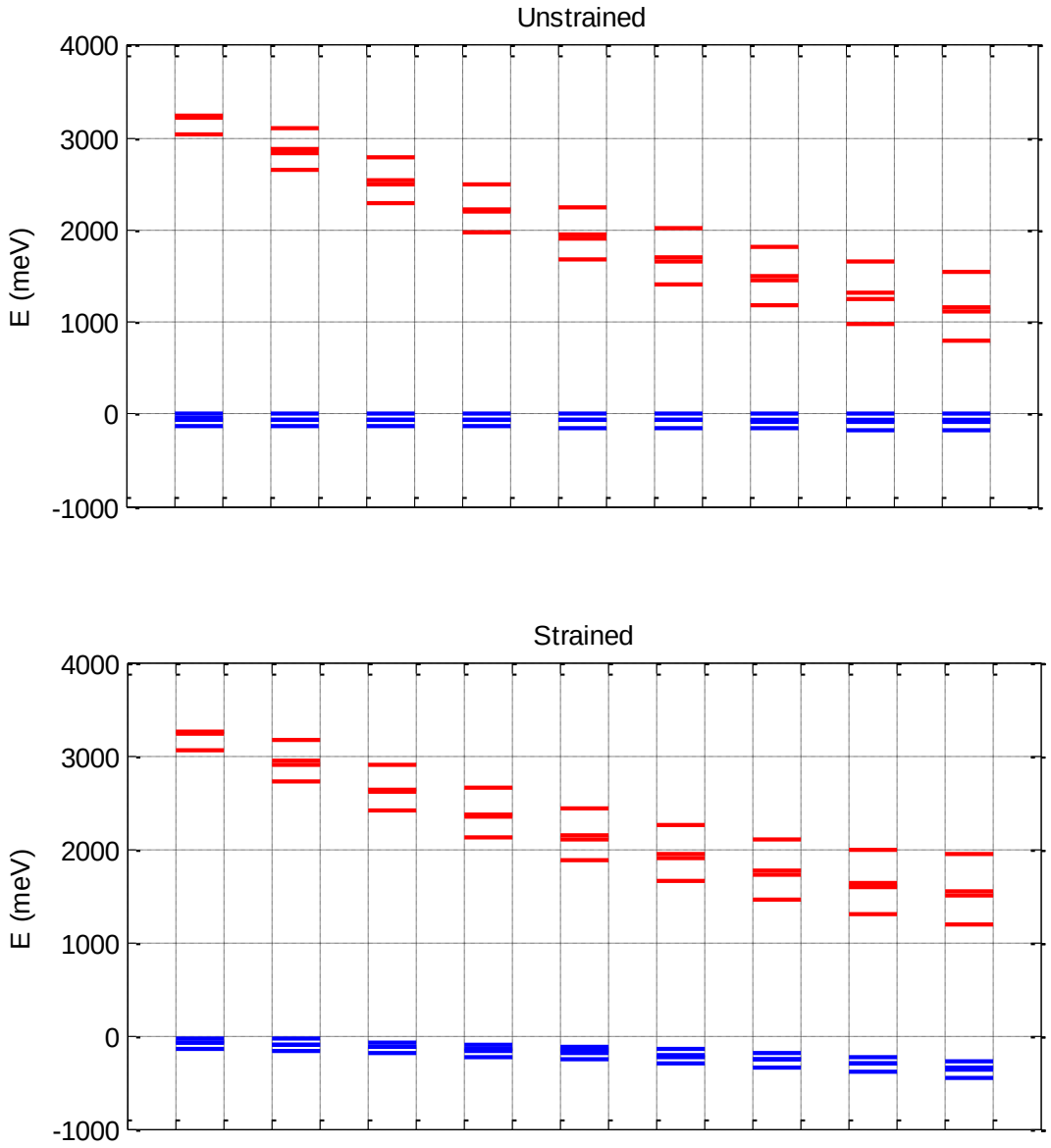

Figure 6 Conduction and valence subbands for $In_xGa_{1-x}N$ / GaN structure with changing In- content in QD, a) Unstrained. b) Strained. Lens shape QD with r=8.5 nm, h=2.2 nm, and elements number Ne=50.

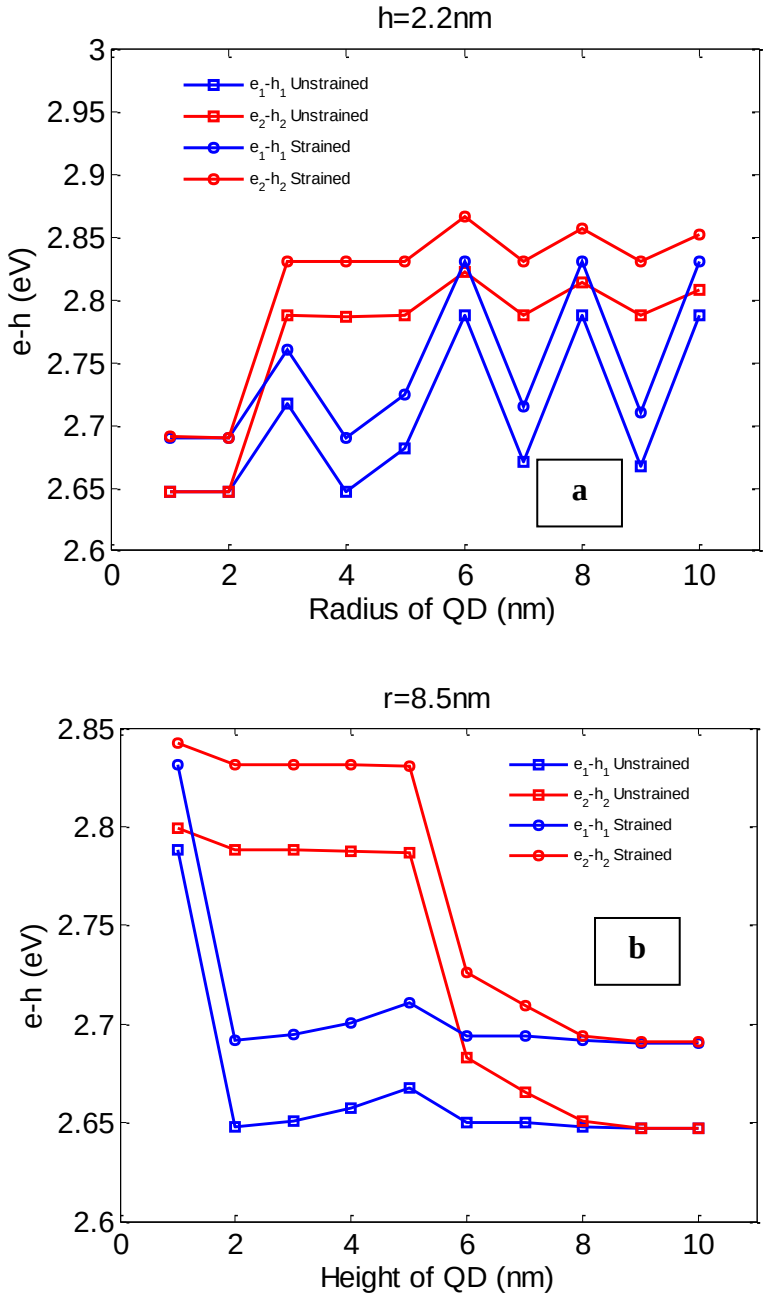

Figure 7 The electron-hole transition energy for GS $(e_1 - h_1)$ and first ES $(e_2 - h_2)$ for LQD as a function of a) QD radius and b) QD height. The structure is $In_{0.2}Ga_{0.8}N$ / GaN.

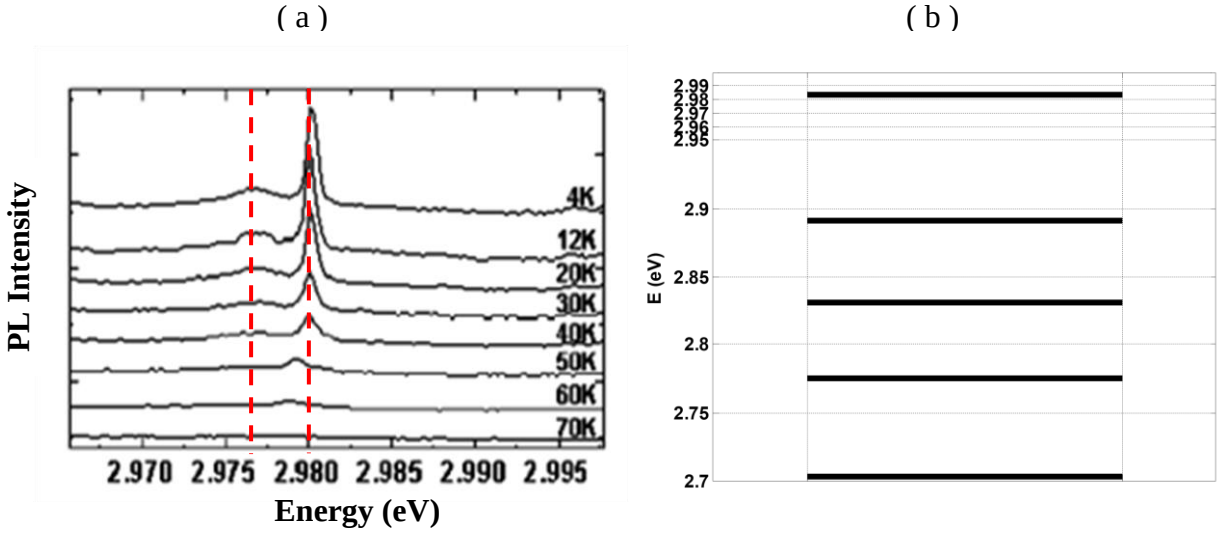

Figure 8 Comparison of our model with experimental results. Left: PL spectrum of the emission from a single QD at various temperatures of $In_{0.2}Ga_{0.8}N/GaN$ structure for LQD size is r=10 nm, h=6 nm [15]. Right: Corresponding calculated subbands.

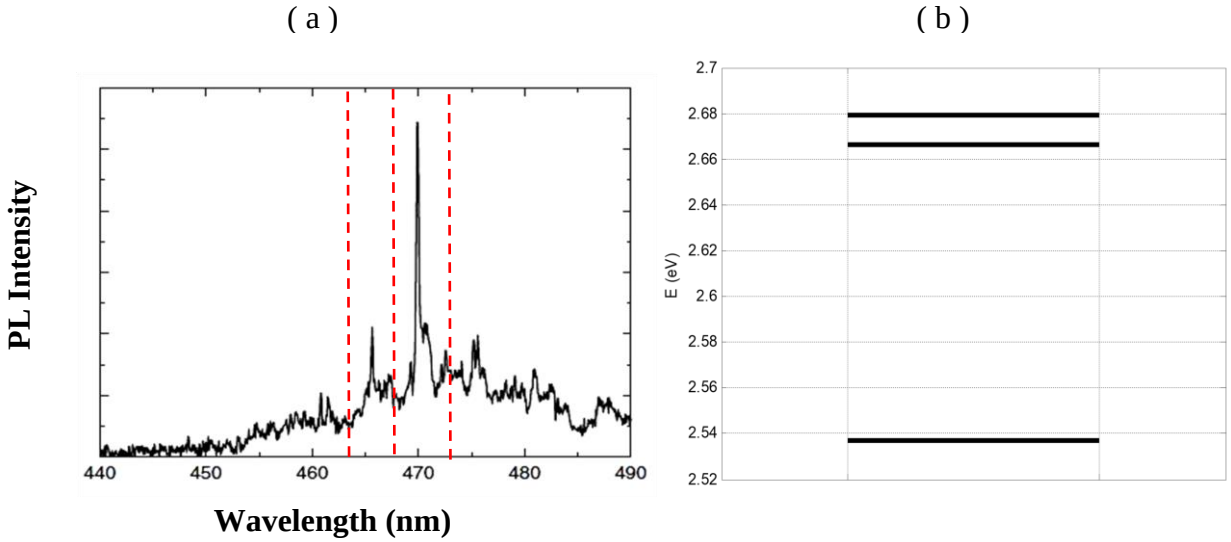

Figure 9 Comparison our model with experimental results. Left: PL spectrum of the emission from a single QD at various temperatures of $In_{0.25}Ga_{0.75}N/GaN$ structure for LQD size is r=15 nm, h=2 nm[16]. Right: Correspond

The main observation is observed from Fig. 9, the reflection spectra is at ambient temperature. It is noticed that the reflection level is determined. The deduced band gap is in good agreement with the reported values [33,34]. The band gap is quite close to the optimum band gap, which indicates that CCTS quaternary alloy nanostructure is promising materials for photovoltaic applications. In this study, the structure of CCTS belongs to the tetragonal crystal system and stannite structure that is in agreement with the standard (ICDD PDF2008, 00-029-0537). The lattice constants (a & c) with other parameters are determined from (112) peak as shown in Table 1.

4. CONCLUSIONS

This work models the electronic structure for different shapes of QDs, thus a Hamiltonian for different QD shapes was introduced. FEM was used to calculate results where the stability of the calculated results was examined. The strain was included in our study and is shown to increase the transition energy of the structures. Mole fraction is also examined for these structures. Our results are comparable with the experimental results.

References

[1] Maksym, P. and T. Chakraborty, Physical review letters, 65 (1990) 108
[2] Jungho, K. and S.-L. Chuang, IEEE Journal of Quantum Electronics 42 (2006) 942
[3] Zhang, L., J.-j. Shi, and H.-j. Xie, Solid State Communications 140 (2006) 549
[4] Nenad, V., et al., Journal of Physics: Condensed Matter 18 (2006) 6249
[5] Saïdi, I., et al., Journal of Applied Physics 109 (2011) 85
[6] Jain, S.C., et al., Journal of Applied Physics 87 (2000) 965
[7] Abraham George, Exp. Theo. NANOTECHNOLOGY 5 (2021) 37
[8] Smith, I.M., D.V. Griffiths, and L. Margetts, Programming the Finite Element Method. 5, revised ed. 2013: John Wiley & Sons.
[9] Jamil, M., et al., Applied Physics Letters 87 (2005) 96
[10] Kapoor, S., J. Kumar, and P.K. Sen, Physica E: Low-dimensional Systems and Nanostructures, 42 (2010) 2380
[11] Negi, C.M.S., et al., Superlattices and Microstructures 60 (2013) 462
[12] Parvizi, R., Physica B: Condensed Matter 456 (2015) 87
[13] Zain A. Muhammad, Tariq J. Alwan, Exp. Theo. NANOTECHNOLOGY 5 (2021) 47
[14] Vurgaftman, I. and J.R. Meyer, Electron Bandstructure Parameters, in Nitride Semiconductor Devices: Principles and Simulation, J. Piprek, Editor. 2007, Wiley-VCH Verlag GmbH & Co. KGaA. p. 13-48.
[15] Aseel I. Mahmood, Shehab A. Kadhim, Nadia F. Mohammed, Intisar A. Naseef, Exp. Theo. NANOTECHNOLOGY 5 (2021) 57
[16] Reid, B.P.L., et al., Japanese Journal of Applied Physics 52 (2013) 08JE01